Materials Research Letters

ISSN: (Print) (Online) Journal homepage: https://www.tandfonline.com/loi/tmrl20

Fe_2C- and $Mn_2(W/Mo)B_4$-based rare-earth-free permanent magnets as a result of the high-throughput and data-mining search

Alena Vishina, O. Eriksson & H. C. Herper

To cite this article: Alena Vishina, O. Eriksson & H. C. Herper (2023) Fe_2C- and $Mn_2(W/Mo)B_4$-based rare-earth-free permanent magnets as a result of the high-throughput and data-mining search, Materials Research Letters, 11:1, 76-83, DOI: 10.1080/21663831.2022.2117576

To link to this article: https://doi.org/10.1080/21663831.2022.2117576

MATER. RES. LETT.
2023, VOL. 11, NO. 1, 76–83
https://doi.org/10.1080/21663831.2022.2117576

MATERIALS RESEARCH LETTERS
Taylor & Francis
Taylor & Francis Group

ORIGINAL REPORTS

Fe_2C- and $Mn_2(W/Mo)B_4$-based rare-earth-free permanent magnets as a result of the high-throughput and data-mining search

Alena Vishina[a], O. Eriksson [a,b] and H. C. Herper [a]

[a]Department of Physics and Astronomy, Uppsala University, Uppsala, Sweden; [b]School of Science and Technology, Örebro University, Örebro, Sweden

ABSTRACT

A high-throughput and data-mining search for rare-earth-free permanent magnets is reported for materials containing a 3*d* and *p*-element of the Periodic Table. Three of the most promising compounds, Fe_2C, Mn_2MoB_4, and Mn_2WB_4, were investigated in detail by ab initio electronic structure theory coupled to atomistic spin-dynamics. For these systems doping protocols were also investigated and, in particular, $(Fe_{0.75}X_{0.25})_2C$ (X = Mn, Cr, V, and Ti), Mn_2XB_4 (X = Mo and W) along with $Mn_2(X_{0.5}Y_{0.5})B_4$ (X,Y = Mo, W, Ta, Cr) are suggested here as promising candidates for applications as permanent magnets.

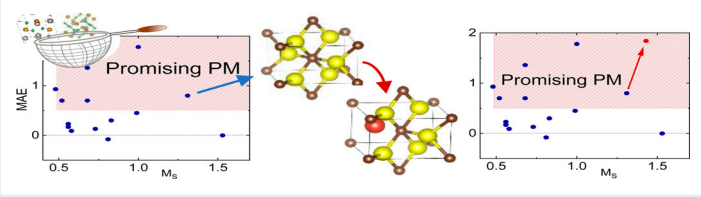

IMPACT STATEMENT

Several promising high-performance rare-earth-free permanent magnets have been found as a result of an ab initio high-throughput search. Alteration proposed to improve their stability and magnetic properties.

ARTICLE HISTORY
Received 25 July 2022

KEYWORDS
Permanent magnet; rare-earth-free; high-throughput; data-mining; DFT

1. Introduction

Permanent magnets (PM) are in high demand for a large number of applications, including electric motors and power generators. These 'green' technology applications have weight and size limitations, hence require high-performance PM with especially high saturation magnetization, high Curie temperature, and large uniaxial magnetic anisotropy (MA). Currently the market is dominated by rare-earth (RE) permanent magnets which significantly outperform their RE-free counterparts. However, there exists a growing interest in finding magnetic materials that are close in performance, yet do not contain RE-elements (such as Pr, Nd, Sm, Tb, or Dy) [1], which are quite expensive and are often mined in environmentally challenging ways. Some of the RE elements (such as Dy that was categorized as the single most critically threatened strategic material [2]) are rapidly decreasing in availability. At the same time, there is a gap between the low-cost hard ferrite magnets with their moderate performance and RE permanent magnets in the price-performance diagram, hence providing a demand on filling this gap with RE-free magnetic materials [3].

Various approaches are currently used to discover and design the RE-free and RE-lean [4–6] magnets with required characteristics. The most widely researched compounds are high magnetocrystalline anisotropy alloys (MnBi [7] and MnAl [8]), $L1_0$ phase of FeNi [9,10], nanostructures [11–13], thin films [14], alnico permanent magnets, and many more [3,15].

Data-mining algorithms have been proposed for some time to be used in search for functional materials. Examples of such studies involve the suggestion of new materials in reduced dimension, particularly two-dimensional (2D) ones [16,17]. Several of these predictions were in fact verified in subsequent works [18–20], demonstrating

CONTACT Alena Vishina alena.vishina@physics.uu.se Department of Physics and Astronomy, Uppsala University, Box 516, SE-75120 Uppsala, Sweden

Supplemental data for this article can be accessed here. https://doi.org/10.1080/21663831.2022.2117576

the power of this type of investigation. It is particularly relevant for the current work that a high-throughput density functional theory (DFT) data-mining approach was proposed in [21] to identify new RE-free permanent magnets and further used to discover a new class of RE-free magnetic materials [22]. In the current investigation we perform data-mining protocols for materials that combine one magnetic element of the 3d series (Cr, Mn, Fe, Co and Ni) and one p-bonded element.

2. Computational methods

A high-throughput search was performed with the full-potential linear muffin-tin orbital method (FP-LMTO), including spin-orbit interaction as implemented in the RSPt code [23,24], with the PBE functional [25] for exchange and correlation. The results were obtained with the tetrahedron method with Blöchl correction for the Brillouin zone integration [26,27]. The initial magnetic state for each compound was assumed to be ferromagnetic (FM).

Magnetic anisotropy energy (MAE) was calculated using the RSPt code as $\Delta E = E^{pl} - E^{c}$; here E^{c} and E^{pl} are the total energies with the magnetization directed along and perpendicular to the c-axis. A positive sign of the MAE corresponds to the required uniaxial anisotropy with preferred magnetization along the c-axis. The converged k-point Monkhorst-Pack meshes [28] $20 \times 20 \times 20$ were used for the calculations.

When different elements are substituted in the materials listed in ICSD, the relaxed crystal structure was determined using Vienna Ab Initio Simulation Package (VASP) [29,30] within the Projector Augmented Wave (PAW) method [31]. Also, GGA in Perdew, Burke, and Ernzerhof (PBE) form [25] was employed for these investigations. The magnetic state of the materials (where not previously known from the literature) was also obtained using VASP by performing the calculations with various initial magnetic moment configurations.

The Curie temperature was determined using Metropolis Monte Carlo (MC) and Atomistic Spin Dynamics (ASD) simulations implemented within the Uppsala Atomistic Spin Dynamics (UppASD) software [32]. The simulations were performed on a $25 \times 25 \times 25$ supercell with periodic boundary conditions using the exchange parameters calculated with the RSPt code within the first nine coordination shells [33–35] and with the PBE functional [25] for exchange and correlation.

Formation enthalpy of a material with respect to its elemental components was calculated using VASP as the energy of the material relative to the composition-weighted average of the energies of the pure constituents. An example of such a calculation is

$$\Delta H[(\mathrm{Fe_xCo_y})_2\mathrm{C}] = E_{(\mathrm{Fe_xCo_y})_2\mathrm{C}} - 2xE_{\mathrm{Fe}} - 2yE_{\mathrm{Co}} - E_{\mathrm{C}}.$$

Here $E_{(\mathrm{Fe_xCo_y})_2\mathrm{C}}$, E_{Fe}, E_{Co}, and E_{C} are the energies of $(\mathrm{Fe}_x\mathrm{Co}_y)_2\mathrm{C}$, body-centered cubic (bcc) iron, hexagonal close-packed (hcp) cobalt, and graphite, respectively. The result described below is then given per atom in a unit cell.

For partial element substitution the spin-polarized relativistic Korringa–Kohn–Rostoker (SPR-KKR) code [36] was also used to obtain the total energies, magnetization, and MAE by solving the Kohn–Sham equations within Green's function formalism. The MAE was then calculated by the torque method [37], however, without considering the full-potential effects, as these calculations employed the atomic sphere approximation (ASA). This method allows to study the electronic structure of a random alloy using the coherent potential approximation (CPA) [38,39]. No lattice relaxation was performed in this case. The PBE [25] approximation was employed as the exchange-correlation functional. The angular momentum cutoff of $l_{\max} = 4$ was used in the multiple scattering expansion. A converged k-point grid was utilized for the magnetization direction dependent self-consistent total energy calculations. In this set of calculations the Curie temperature was calculated within the mean-field approximation [40] based on the ferromagnetic reference state.

In addition, the Sumo package [41] and VESTA code [42] were utilized for visualization.

3. Results

3.1. High-throughput search

Similar to previous investigations [21,22], the current work is based on a high-throughput search performed among the materials listed in the ICSD database [43]. Filtering through the systems that contain a magnetic 3d-element (Cr, Mn, Fe, Co, Ni) and an element of the p-block (oxygen and noble gases excluded) up to Bi (see Figure 1), we data-mined among several thousands of compounds to find materials with ferromagnetic ordering, a high saturation magnetization ($M_S > 0.5$ T), a Curie temperature T_C above 400 K, and a large uniaxial MAE (> 0.5 MJ/m^3) (for the details see [21] and the *Computational methods* section). We made sure that all the materials already considered in [21,22] were excluded from the search. As in the previous studies, initially, oxides, rare-earth materials, alloys, and materials with cubic symmetry were not considered [21]. In addition, the maximum number of atoms per unit cell was limited

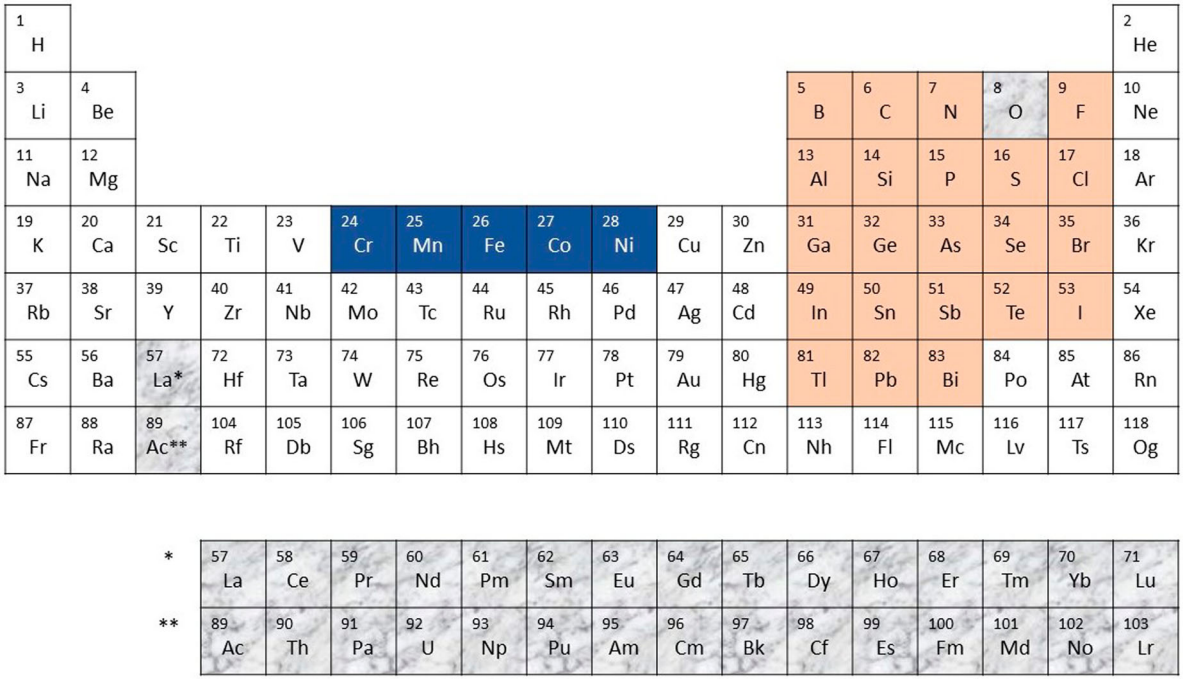

Figure 1. The elements of the Periodic Table necessarily included in the initial choice—magnetic 3d-elements (dark blue) and the elements of the p-block (orange). The search excluded the compounds containing oxygen and rare-earths (marble colored).

to 40. At this point, the initial set consisted of 559 systems. The first high-throughput step left 166 compounds with sufficiently large magnetic moment (note that in our setup we start with a ferromagnetic initial configuration). A careful literature search was performed here; many of the structures were known from previous experimental investigations to be either established magnetic materials or even antiferromagnets. For the remaining systems, the ground state magnetic configuration and magnetocrystalline anisotropy were determined. The results are given in Figure 2 with focus on saturation field and magnetic anisotropy (for more details see the *Supplementary materials*, where the ordering temperatures are listed as well). As seen from the figure, the values of saturation magnetization and magnetic anisotropy energy are comparable to several well-known PM. One may note that several new materials of Figure 2 show magnetic performance that are close to what is needed for practical use as a PM.

In addition to the high-throughput search, we optimized the performance of several of the most promising candidates. The class of materials shown in Figure 2 can typically be improved with respect to their stability and magnetic qualities, primarily by a full or partial element substitution with the neighboring elements of the Periodic Table.

In this work, we consider in particular three systems that were obtained in the high-throughput search and are of special interest for the permanent magnet applications: Fe_2C, Mn_2MoB_4, and Mn_2WB_4. Each system is investigated in detail below, with emphasis on improving their magnetic characteristics for applications as PM. Iron–carbon compounds have attracted some attention recently as interesting candidates for permanent magnets applications [44–46], while 4d and 5d transition elements are known to provide large MA due to the strong spin-orbit coupling [47,48].

3.2. Fe_2C

The unit cell of Fe_2C (ICSD 76826) with the *Pnnm* (58) space group is shown in Figure 3. According to our calculations, Fe_2C has a saturation magnetization of 1.31 T, a magnetic anisotropy energy equal to 0.80 MJ/m^3, and a high T_C of 900 K. The carbide was reported to be prepared and studied by electron microscopy in [49]. The structural and electronic properties of metastable monoclinic Fe_2C, also known as η-Fe_2C, have been previously investigated in [44,45]; the stability was shown to be poor, and the value of magnetization was found to be very close to the one we reported here. η-Fe_2C is one of the transition carbides formed in steels tempered at different temperatures [49]. It is precipitated during the first stage of tempering of martensitic high carbon steel. The type of the carbide formed depends on tempering time, the temperature range, and an external field [44]. It was shown in [44,45] that η-Fe_2C is more stable than χ-Fe_2C and ϵ-Fe_2C. η-Fe_2C can also be obtained by high-fluence ion implantation [50].

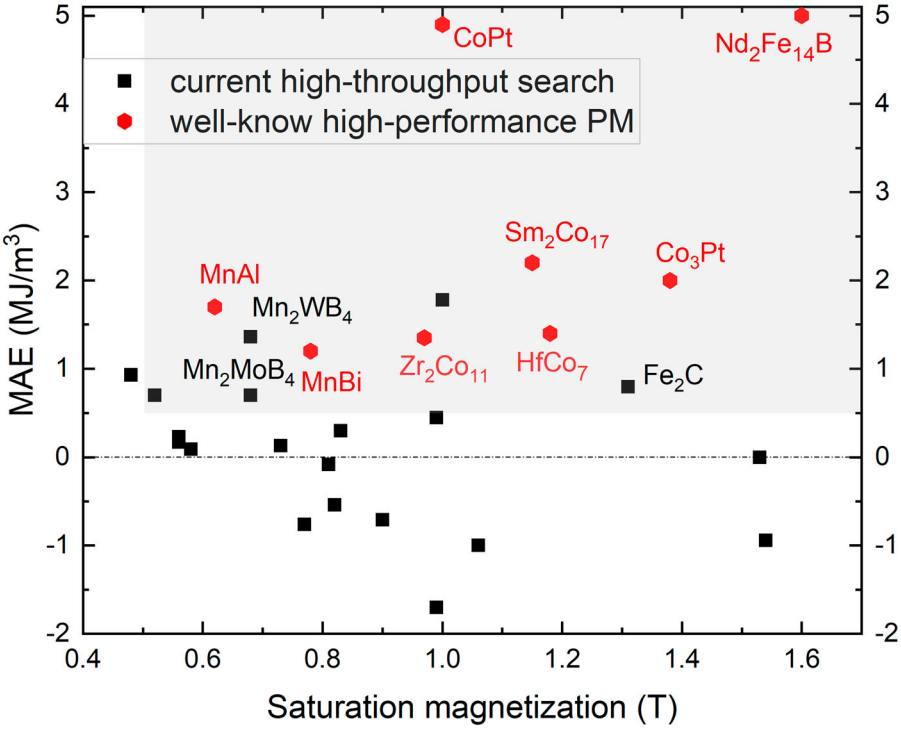

Figure 2. The distribution of saturation magnetization vs MAE for the materials found in the current high-throughput search that are FM and possess a high enough magnetic moment. Several values for the known high-performance PM are given for comparison (red dots). The grey rectangle contains the materials that fulfill the desired search criteria without additional alloying.

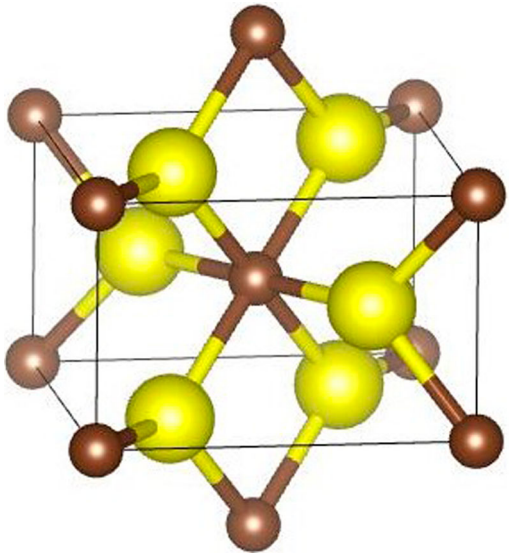

Figure 3. The unit cell of Fe_2C. Iron atoms are shown with the large yellow spheres, C atoms are small dark brown spheres. The *c*-axis is pointing upwards.

To investigate if the phase stability of Fe_2C can be improved without influencing the promising magnetic properties, we replaced one out of four Fe atoms of the unit cell with Co, Mn, Cr, V, and Ti. The crystal structure of $(Fe_{0.75}Co_{0.25})_2C$, $(Fe_{0.75}Mn_{0.25})_2C$, $(Fe_{0.75}Cr_{0.25})_2C$, $(Fe_{0.75}V_{0.25})_2C$, and $(Fe_{0.75}Ti_{0.25})_2C$ was optimized using VASP (for details see the *Computational methods* section). All iron atoms in the unit cell are equivalent, hence checking for the most likely substitution position was not necessary. However, we relaxed the structures both with the initial FM and AFM spin configurations to make sure that the ferromagnetic spin orientation is still preferable. The values of saturation magnetization, MAE, and Curie temperature for the relaxed compounds are given in Table 1.

Table 1. Saturation magnetization, MAE, Curie temperature, and enthalpy of formation for $(Fe_{0.75}X_{0.25})_2C$, with X = Co, Mn, Cr, V, and Ti. T_C was calculated only for the materials with high MAE. Values for the parent compound Fe_2C are also given for comparison.

	Magnetic	MAE	Sat. magn.,	T_C	ΔH
X	state	(MJ/m^3)	(T)	(K)	(mEv/at)
Co	FM	0.21	1.08		76
Mn	FM	1.84	1.43	950	−4.85
Cr	FM	1.34	1.10	730	39
V	FM	1.01	0.82	650	−52
Ti	FM	0.51	0.64	400	−132
Fe_2C	FM	0.80	1.31	900	49.7

As seen from Table 1, Co and Ti substitution resulted in a substantial drop in magnetization and MAE, and for the reason we did not evaluate the ordering temperature for $(Fe_{0.75}Co_{0.25})_2C$. For the remaining materials, $(Fe_{0.75}Cr_{0.25})_2C$, $(Fe_{0.75}Mn_{0.25})_2C$, and $(Fe_{0.75}V_{0.25})_2C$, the T_C was computed and found to remain high.

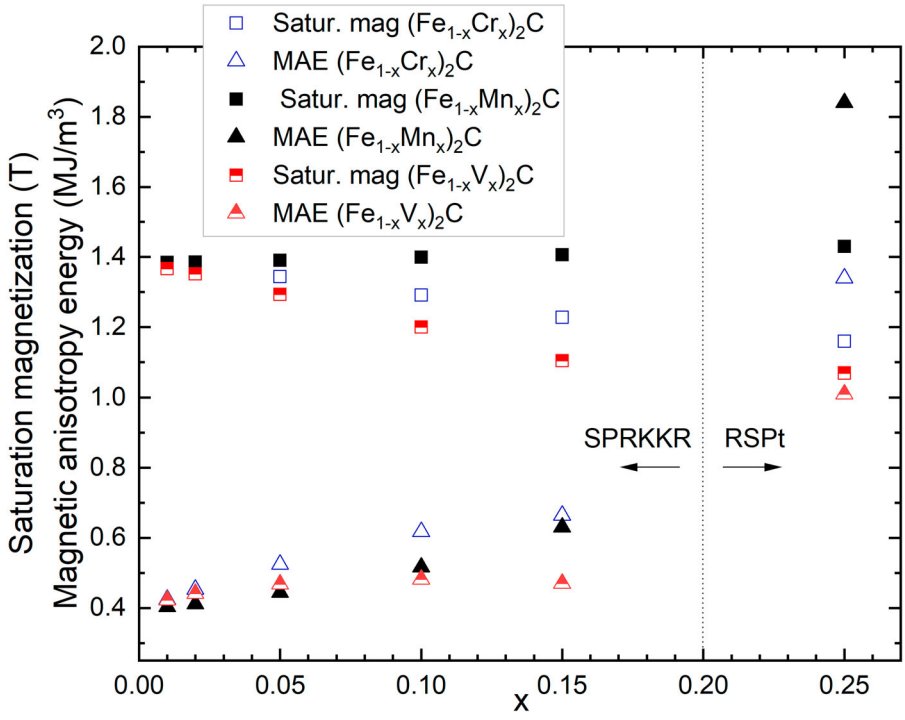

Figure 4. Saturation magnetization and MAE calculated for Fe_2C doped with V, Cr, and Mn. Left-hand side of the graph shows the result obtained with SPRKKR in CPA. The right-hand side points are supercell calculations in RSPt for $(Fe_{0.75}X_{0.25})_2C$.

We calculated also the formation enthalpy of $(Fe_{0.75}X_{0.25})_2C$, with X = Co, Mn, Cr, V, and Ti (see Table 1). For comparison, the formation enthalpy of Fe_2C was also computed (49.7 meV/atom). The positive value of the formation enthalpy means that the phase is unstable at low temperature (0 K in our calculations). According to the data in Table 1, adding manganese, chromium, vanadium, and titanium makes the formation enthalpy negative (meaning that the phase is stable) or produces a less positive value. Hence, doping Fe_2C with manganese, chromium, vanadium, and titanium is expected to produce a more stable phase, while maintaining good magnetic properties.

In order to study the influence of low concentrations of impurities, we made use of the CPA as implemented in the SPRKKR code (for details see *Computational methods* section)). Using this method we analyzed the effect of Mn, Cr, and V alloying in the range 0–15 % substitution. Since small amounts of dopants were considered, we kept the experimental crystal structure parameters of Fe_2C. The outcome is shown in Figure 4 and one can observe that the results obtained from the CPA method, as given by the SPRKKR code, are consistent with supercell results obtained from the RSPt code—the saturation magnetization (as one would expect) decreases as more Fe is replaced by Cr or V, while replacing Fe for Mn produces a rather concentration independent saturation magnetization. Furthermore, the figure shows that adding V, Cr, and Mn increases the MAE compared to the value of Fe_2C.

One may see in Figure 4 that the supercell calculations with the FP-LMTO code RSPt agree well with the CPA calculations performed with the SPRKKR code, particularly concerning the magnetic moment of the $(Fe_{0.75}X_{0.25})_2C$ compounds. The MAE calculated with RSPt is slightly higher than the result given by SPR-KKR. However, the numbers agree qualitatively both for on the sign and order of magnitude. The origin of magnetic anisotropy is analyzed in more detail in the *Supplementary materials*.

3.3. Mn_2MoB_4 and Mn_2WB_4

Mn_2MoB_4 was reported in [51] as well as in [52], where it was investigated amongst the Mn_2XB_4 (X = Mo, W, Ta, Cr) compounds. The unit cell of Mn_2WB_4 (ICSD 614782, space group *Immm* (71)) is shown in Figure 5. Mn_2CrB_4 did not appear in our high-throughout search since it is not in the ICSD database. However, as it can be found in [52], it will be investigated here (see Table 2).

In some cases we also considered alloys between systems that in pure form were found unsuitable, but where alloying may produce a material with desired properties. For instance, Mn_2TaB_4 has an in-plane magnetic

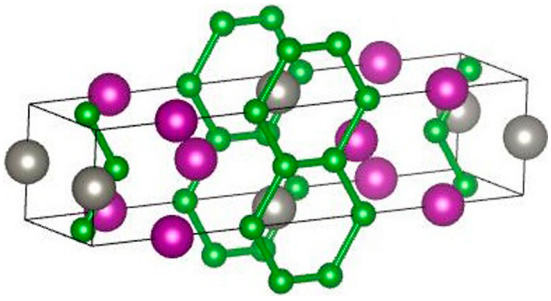

Figure 5. The unit cell of Mn_2WB_4. Manganese atoms are shown with the purple spheres, B atoms are green, and W atoms are gray.

Table 2. Curie temperature and saturation magnetization both calculated (in this work) and measured in [52] for Mn_2XB_4 (X = Mo, W, Ta, Cr) compounds, as well as calculated MAE. The second half of the tables provides the same numbers calculated for $Mn_2(X_{0.5}Y_{0.5})B_4$ structures (X,Y = Mo, W, Ta, Cr).

	$T_{C,th}$	$T_{C,exp}$	MAE	$M_{S,th}$	$M_{S,exp}$
X/Y	(K)	(K), [52]	$(MJ/m)^3$	(T)	(T) [52]
Mo	630	590	0.70	0.68	0.53
W	610	575	1.36	0.68	0.45
Ta	1080	780	−0.74	0.77	0.55
Cr	950	440	0.70	0.70	0.55
Cr/Mo	740		0.52	0.68	
Mo/Ta	850		0.18	0.71	
W/Mo	800		1.15	0.67	
W/Ta	830		1.06	0.72	

anisotropy (see Table 2), but an alloy of $Mn_2(X_{0.5}Y_{0.5})B_4$ form (X,Y = Mo, W, Ta, Cr) may be interesting, since the Ta-based compound with its planar anisotropy has the highest Curie temperature according to the experimental data, while the W-based material has the highest MAE (see Table 2). The supercell approach was used for these systems to investigate the materials of $Mn_2(X_{0.5}Y_{0.5})B_4$ form (X,Y = Mo, W, Ta, Cr); the initial unit cell with one X/Y atom per unit cell was doubled, the crystal structure relaxed with VASP, and their magnetic properties calculated.

Mn_2CrB_4 is not in the ICSD database, and we considered this new compound by first optimizing its structural parameters, and then we obtained its MAE, saturation magnetization, and Curie temperature. All of the values calculated for Mn_2XB_4 compounds using RSPt and UppASD codes are given in Table 2 along with the experimental data [52].

The values of the relevant magnetic properties can be found in Table 2. As all the initial compounds have similar magnetic moment, the value of M_S unsurprisingly does not change much. The MAE of $Mn_2(X_{0.5}Y_{0.5})B_4$ is close to an average of its values in Mn_2XB_4 and Mn_2YB_4 for each combination of *X* and *Y*. Hence, the systems containing tungsten have the highest magnetic anisotropy, while adding tantalum improves the Curie temperature but causes the drop in MAE.

4. Discussion and conclusions

As a result of the high-throughput, data-mining search for RE-free permanent magnets, several promising candidates are reported here. The focus of the investigation is on systems with 3*d* elements and a *p*-element. Several of the materials identified here have magnetic properties that make them suitable for permanent magnet applications. One, Fe_2C (ICSD 76826), has a high magnetization of 1.31 T, MAE of 0.8 MJ/m^3, and a Curie temperature of 900 K. Unfortunately, it is known to have poor chemical stability. As can be seen from Table 1, both magnetic characteristics and stability of Fe_2C can be improved by doping. The border of a 'metastable' state, or the 'instability' energy which allows the material to be made, is usually considered to be 40–50 meV/atom [53,54]. With this in mind, out of the five dopants investigated here, Mn, Cr, V, Ti, are the most promising candidates.

Also, $(Fe_{0.75}Ti_{0.25})_2C$, even though it has lower magnetization than Fe_2C, has the lowest formation enthalpy. Alloying with Mn seems the most promising from the magnetic side of things, as it increases saturation magnetization to 1.84 T, MAE to 1.43 MJ/m^3, and the Curie temperature to 950 K, while the formation enthalpy of $(Fe_{0.75}Mn_{0.25})_2C$ is still slightly negative. Adding vanadium can be considered the best of two worlds, as $(Fe_{0.75}V_{0.25})_2C$ has decent magnetic qualities and low formation enthalpy.

The advantage of Mn_2XB_4 (X = Mo, W, Ta, Cr) compounds is that these are known stable phases. According to the calculations presented here, the materials have similar saturation magnetization. Mn_2CrB_4 has the highest Curie temperature (out of the compounds with uniaxial magnetic anisotropy) while Mn_2WB_4 has the highest MAE. Table 2 shows the comparison between experimental and theoretical data. The material where theory fails to reproduce the experiment is Mn_2CrB_4. This discrepancy, however, can be explained by the experimental details reported in [55]. The authors observed several phases (FM and AFM) coexisting in the sample depending on the concentration of Cr, which affected the measured magnetic properties.

To improve on the properties of these materials, we considered the combinations of $Mn_2(X_{0.5}Y_{0.5})B_4$ form (X,Y = Mo, W, Ta, Cr). From the second half of Table 2 one may note that combining W with Mo, and W with Ta produces the best result. Both have a T_C above 800 K, a saturation magnetization higher than 0.5 T, and a MAE above 1.0 MJ/m^3. Magnetization here is not high enough to compete with the best known RE permanent

magnets. However, it does allow to fill the gap between the high-performance RE and the weak RE-free PM.

Hence, employing the high-throughput and data-mining searches for RE-free PM we identified several promising materials and suggested a number of chemical substitutions that can improve their magnetic properties. In particular, $(Fe_{0.75}X_{0.25})_2C$ (X = Mn, Cr, V, and Ti), Mn_2XB_4 (X = Mo and W) along with $Mn_2(X_{0.5}Y_{0.5})B_4$ (X,Y = Mo, W, Ta, Cr) are suggested here as promising candidates for applications as permanent magnets.

Disclosure statement

No potential conflict of interest was reported by the author(s).

Funding

The computations were enabled by resources provided by the Swedish National Infrastructure for Computing (SNIC) partially funded by the Swedish Research Council through grant agreement no. 2018-05973 (SNIC 2022/5-338, SNIC 2021/1-36), and UPPMAX (SNIC 2021/5-340). Also the Knut and Alice Wallenberg Foundation (KAW), eSSENCE, STandUPP, and the ERC supported this work.

ORCID

O. Eriksson http://orcid.org/0000-0001-5111-1374
H. C. Herper http://orcid.org/0000-0001-6159-1244

References

[1] Skomski R, Coey JMD. Permanent magnetism. Bristol: Institute of Physics Publishing; 1999.
[2] Bauer D, Diamond D, Li J, et al. US department of energy: critical materials strategy; 2010.
[3] Cui J, Kramer M, Zhou L, et al. Current progress and future challenges in rare-earth-free permanent magnets. Acta Mater. 2018;158:118–137. Available from: http://www.sciencedirect.com/science/article/pii/S1359645418305858.
[4] Sözen HI, Ener S, Maccari F, et al. Ab initio phase stabilities of ce-based hard magnetic materials and comparison with experimental phase diagrams. Phys Rev Materials. 2019;3:084407. Available from: https://link.aps.org/doi/10.1103/PhysRevMaterials.3.084407.
[5] Pandey T, Parker DS. Potential high-performance magnet: Fe- and Zr-alloyed ce_2co_{17}. Phys Rev Appl. 2020;13:034039. Available from: https://link.aps.org/doi/10.1103/PhysRevApplied.13.034039.
[6] Gilad Kusne A, Gao T, Mehta A, et al. On-the-fly machine-learning for high-throughput experiments: search for rare-earth-free permanent magnet. Sci Rep. 2014;4:6367.
[7] Gabay A, Hadjipanayis G, Cui J. New anisotropic MNBI permanent magnets by field-annealing of compacted melt-spun alloys modified with Mg and Sb. J Magn Magn Mater. 2020;495:165860. Available from: http://www.sciencedirect.com/science/article/pii/S0304885319322632.
[8] Fang H, Kontos S, Ångström J, et al. Directly obtained τ-phase MNAL, a high performance magnetic material for permanent magnets. J Solid State Chem. 2016;237:300–306. Available from: http://www.sciencedirect.com/science/article/pii/S0022459616300548.
[9] Tian L, Gutfleisch O, Eriksson O. Alloying effect on the order–disorder transformation in tetragonal feni. Sci Rep. 2021;11:5253. https://doi.org/10.1038/s41598-021-84482-53.
[10] Takanashi K, Mizuguchi M, Kojima T, et al. Fabrication and characterization of $l1_0$-ordered feni thin films. J Phys D: Appl Phys. 2017;50(48):483002. https://doi.org/10.1088/1361-6463/aa8ff6.
[11] Lottini E, López-Ortega A, Bertoni G, et al. Strongly exchange coupled core-shell nanoparticles with high magnetic anisotropy: a strategy toward rare-earth-free permanent magnets. Chem Mater. 2016;28(12):4214.
[12] Balamurugan B, Das B, Shah VR, et al. Assembly of uniaxially aligned rare-earth-free nanomagnets. Appl Phys Lett. 2012;101:122407.
[13] Mohapatra J, Xing M, Elkins J, et al. Extraordinary magnetic hardening in nanowire assemblies: the geometry and proximity effects. Adv Funct Mater. 2021;31(13):2010157.
[14] Gao TR, Wu YQ, Fackler S, et al. Combinatorial exploration of rare-earth-free permanent magnets: magnetic and microstructural properties of Fe-Co-W thin films. Appl Phys Lett. 2013;102:022419.
[15] Kuz'min MD, Skokov KP, Jian H, et al. Towards high-performance permanent magnets without rare earths. J Phys: Condensed Matter. 2014;26(6):064205.
[16] Lebègue S, Björkman T, Klintenberg M, et al. Two-dimensional materials from data filtering and ab initio calculations. Phys Rev X. 2013;3:031002. Available from: https://link.aps.org/doi/10.1103/PhysRevX.3.031002.
[17] Eriksson O. Searching for materials with reduced dimension. Nature Nanotech. 2017;13:180. https://doi.org/10.1038/s41565-017-0060-4.
[18] Romdhane FB, Cretu O, Debbichi L, et al. Quasi-2d Cu_2s crystals on graphene: in-situ growth and ab-initio calculations. Small. 2015;11(11):1253–1257. Available from: https://onlinelibrary.wiley.com/doi/abs/10.1002/smll.201400444.
[19] Lin MW, Zhuang HL, Yan J, et al. Ultrathin nanosheets of $crsite_3$: a semiconducting two-dimensional ferromagnetic material. J Mater Chem C. 2016;4:315–322. http://dx.doi.org/10.1039/C5TC03463A.
[20] Nieves P, Arapan S, Maudes-Raedo J, et al. Database of novel magnetic materials for high-performance permanent magnet development. Comput Materials Sci. 2019;168:188–202. Available from: https://www.sciencedirect.com/science/article/pii/S0927025619303489.
[21] Vishina A, Vekilova OY, Björkman T, et al. High-throughput and data-mining approach to predict new rare-earth free permanent magnets. Phys Rev B. 2020 Mar;101:094407. Available from: https://link.aps.org/doi/10.1103/PhysRevB.101.094407.
[22] Vishina A, Hedlund D, Shtender V, et al. Data-driven design of a new class of rare-earth free permanent magnets. Acta Mater. 2021;212:116913. Available from:

https://www.sciencedirect.com/science/article/pii/S1359645421002937.
[23] Wills JM, Cooper BR. Synthesis of band and model hamiltonian theory for hybridizing cerium systems. Phys Rev B. 1987;36:3809.
[24] Wills JM, Alouani M, Andersson P, et al. Full-potential electronic structure method. Berlin: Springer; 2010. (Springer Series in Solid State Science).
[25] Perdew J, Burke K, Ernzerhof M. Generalized gradient approximation made simple. Phys Rev Lett. 1996;77:3865.
[26] Blöchl PE, Jepsen O, Andersen OK. Improved tetrahedron method for Brillouin-zone integrations. Phys Rev B. 1994;49:16223.
[27] Jepson O, Anderson O. The electronic structure of h.c.p. ytterbium. Solid State Commun. 1971;9(20):1763–1767. Available from: https://www.sciencedirect.com/science/article/pii/0038109871903139.
[28] Monkhorst HJ, Pack JD. Special points for Brillouin-zone integrations. Phys Rev B. 1976;13:5188–5192.
[29] Kresse G, Hafner J. Ab initio molecular dynamics for liquid metals. Phys Rev B. 1993;47:558.
[30] Kresse G, Furthmüller J. Efficiency of ab-initio total energy calculations for metals and semiconductors using a plane-wave basis set. Comput Mat Sci. 1996;6:15–50.
[31] Blöchl PE. Projector augmented-wave method. Phys Rev B. 1994;50:17953–17979.
[32] Eriksson O, Bergman A, Bergqvist L, et al. Atomistic spin dynamics: foundations and applications. Oxford: Oxford University Press; 2017.
[33] Kvashnin YO, Grånäs O, Di Marco I, et al. Exchange parameters of strongly correlated materials: extraction from spin-polarized density functional theory plus dynamical mean-field theory. Phys Rev B. 2015;91:125133. Available from: https://link.aps.org/doi/10.1103/PhysRevB.91.125133.
[34] Liechtenstein AI, Katsnelson MI, Gubanov VA. Exchange interactions and spin-wave stiffness in ferromagnetic metals. J Phys F: Metal Phys. 1984;14(7):L125–L128. https://doi.org/10.1088/0305-4608/14/7/007.
[35] Szilva A, Kvashnin Y, Stepanov EA, et al. Quantitative theory of magnetic interactions in solids, 2022. Available from: https://arxiv.org/abs/2206.02415.
[36] Ebert H, Ködderitzsch D, Minár J. Calculating condensed matter properties using the kkr-green's function method–recent developments and applications. Rep Progress Phys. 2011;74(9):096501. Available from: http://stacks.iop.org/0034-4885/74/i=9/a=096501.
[37] Wang X, Wu R, Wang DS, et al. Torque method for the theoretical determination of magnetocrystalline anisotropy. Phys Rev B. 1996 Jul;54:61–64. Available from: https://link.aps.org/doi/10.1103/PhysRevB.54.61.
[38] Soven P. Coherent-potential model of substitutional disordered alloys. Phys Rev. 1967;156:809–813. Available from: https://link.aps.org/doi/10.1103/PhysRev.156.809.
[39] Stocks GM, Temmerman WM, Gyorffy BL. Complete solution of the Korringa–Kohn–Rostoker coherent-potential-approximation equations: Cu-Ni alloys. Phys Rev Lett. 1978;41:339–343. Available from: https://link.aps.org/doi/10.1103/PhysRevLett.41.339.
[40] Anderson PW. Theory of magnetic exchange interactions: exchange in insulators and semiconductors. In: Seitz F, Turnbull, editors. Solid state physics. New York (NY): Academic Press; 1963.
[41] Ganose A, Jackson A, Scanlon D. Command-line tools for plotting and analysis of periodic ab initio calculations. J Open Source Softw. 2018;3(28):717.
[42] Momma K, Izumi F. *VESTA3* for three-dimensional visualization of crystal, volumetric and morphology data. J Appl Crystallogr. 2011 Dec;44(6):1272–1276. https://doi.org/10.1107/S0021889811038970.
[43] Inorganic crystal structure database. Available from: http://www2.fiz-karlsruhe.de/icsd_home.html; 2021.
[44] Faraoun HI, Zhang YD, Esling C, et al. Crystalline, electronic, and magnetic structures of θ-fe_3c, χ-fe_5c_2, and η-fe_2c from first principle calculation. J Appl Phys. 2006;99(9):093508. https://doi.org/10.1063/1.2194118.
[45] Lv Z, Sun S, Jiang P, et al. First-principles study on the structural stability, electronic and magnetic properties of fe_2c. Comput Mater Sci. 2008;42(4):692–697. Available from: https://www.sciencedirect.com/science/article/pii/S0927025607003084.
[46] Yin L, Juneja R, Lindsay L, et al. Semihard iron-based permanent-magnet materials. Phys Rev Appl. 2021;15:024012. Available from: https://link.aps.org/doi/10.1103/PhysRevApplied.15.024012.
[47] Edström A, Werwiński M, Iuşan D, et al. Magnetic properties of $(Fe_{1-x}Co_x)_2B$ alloys and the effect of doping by 5*d* elements. Phys Rev B. 2015;92:174413. Available from: https://link.aps.org/doi/10.1103/PhysRevB.92.174413.
[48] Bhandary S, Grånäs O, Szunyogh L, et al. Route towards finding large magnetic anisotropy in nanocomposites: application to a $W_{1-x}Re_x$/Fe multilayer. Phys Rev B. 2011;84:092401. Available from: https://link.aps.org/doi/10.1103/PhysRevB.84.092401.
[49] Hirotsu Y, Nagakura S. Crystal structure and morphology of the carbide precipitated from martensitic high carbon steel during the first stage of tempering. Acta Metallurgica. 1972;20(4):645–655. Available from: https://www.sciencedirect.com/science/article/pii/0001601607290020X.
[50] Königer A, Hammerl C, Zeitler M, et al. Formation of metastable iron carbide phases after high-fluence carbon ion implantation into iron at low temperatures. Phys Rev B. 1997;55:8143–8147. Available from: https://link.aps.org/doi/10.1103/PhysRevB.55.8143.
[51] Buschow KHJ, van Engen PG, Jongebreur R. Magneto-optical properties of metallic ferromagnetic materials. J Magn Magn Mater. 1983;38(1):1–22. Available from: https://www.sciencedirect.com/science/article/pii/0304885383900975.
[52] Iga A, Tawara Y. Magnetic properties of molybdenum- and wolfram-modified mn3b4. J Phys Soc Japan. 1968;24(1):28–35. https://doi.org/10.1143/JPSJ.24.28.
[53] Hinuma Y, Hatakeyama T, Kumagai Y, et al. Discovery of earth-abundant nitride semiconductors by computational screening and high-pressure synthesis. Nat Commun. 2016;7:11962.
[54] Wu Y, Lazic P, Hautier G, et al. First principles high throughput screening of oxynitrides for water-splitting photocatalysts. Energy Environ Sci. 2013;6:157–168.
[55] Tawara Y, Iga A, Yanase A. Ferro- and antiferromagnetism in $(Mn_{1-x}Cr_x)_3B_4$. J Phys Soc Japan. 1966;21(3):476–479. https://doi.org/10.1143/JPSJ.21.476.